Surface Science 604 (2010) 1073–1081

Contents lists available at ScienceDirect

Surface Science

journal homepage: www.elsevier.com/ locate/susc

Relative reactivities of amino and ethenyl groups in allylamine on Si(100)2×1: Temperature-dependent X-ray photoemission and thermal desorption studies of a common linker molecule

A. Radi, M. Ebrahimi, K.T. Leung *

WATLab, and Department of Chemistry, University of Waterloo, Waterloo, Ontario, Canada N2L3G1

ARTICLE INFO

Article history:
Received 21 September 2009
Accepted 10 March 2010
Available online 20 March 2010

ABSTRACT

The room-temperature adsorption and thermal evolution of allylamine on Si(100)2×1 have been investigated by using temperature-dependent X-ray photoelectron spectroscopy (XPS) and thermal desorption spectrometry (TDS). The presence of a broad N 1 s feature at 398.9 eV, attributed to a N—Si bond, indicates N—H dissociative adsorption. On the other hand, the presence of C 1 s features at 284.6 eV and 286.2 eV, corresponding to C=C and C—N, respectively, and the absence of the Si—C feature expected at 283.2 eV shows that [2+2] C=C cycloaddition does not occur at room temperature. These XPS data are consistent with the unidentate staggered and eclipsed allylamine conformer adstructures arising from N—H dissociation and not [2+2] C=C cycloaddition. The apparent conversion of the N 1 s feature for Si—N(H)—C← at 398.9 eV to that for Si—N(H) at 397.7 eV and the total depletion of C 1 s feature for C—N at 286.2 eV near 740 K indicates cleavage of the C—N bond, leaving behind a Si—N(H)• radical. Furthermore, the C=C C 1 s feature at 284.6 eV undergoes steep intensity reduction between 740 K and 825 K, above which a new C 1 s feature at 283.2 eV corresponding to SiC is found to emerge. These spectral changes suggest total dissociation of the ethenyl fragment and the formation of SiC. Moreover, while the total N 1 s intensity undergoes a minor reduction (24%) upon annealing up to 1090 K, a considerable reduction (43%) is found in the overall C 1 s intensity. This observation is consistent with our TDS data, which shows the desorption of C-containing molecules including propene and ethylene at 580 K and of acetylene at 700 K. The lack of N-containing desorbates suggests that the dissociated N species are likely bonded to multiple surface Si atoms or diffused into the bulk. Interestingly, both the staggered and eclipsed N—H dissociative adstructures are found to have a less negative adsorption energy than the [N, C, C] tridentate or the [2+2] C=C cycloaddition adstructures by our DFT calculations, which suggests that the observed formation of N—H dissociative adstructures is kinetically favored on the Si(100)2×1 surface.

1. Introduction

Chemisorption of an organic molecule on a solid surface has been an important topic in numerous applications. In particular, the surface provides selectivity and catalytic activity in controlling how the molecule binds to the surface, which in turn adds new functionalities to the resulting adsorbate–substrate configuration [1–3]. These new surface functionalities could lead to better optimized surface properties, elimination of defects or undesirable characteristics, and/or introduction of totally new functions [4]. Si(100)2×1 has been one of the most important substrates in the semiconductor industry. In the generally accepted asymmetric buckled dimer model for the Si(100)2×1 surface, one of the two dangling bonds of a surface atom combines with one other dangling bond of a neighboring atom, forming a strong σ bond, while the remaining dangling bonds of the dimer pair in effect produces a weak π bond [5]. At room temperature, thermal motion causes the resulting dimer to dynamically tilt, giving rise to the buckled dimer [6]. Partial charge transfer from the down-atom to the up-atom of the buckled dimer produces an electrophilic–nucleophilic pair (or a Lewis acid–Lewis base pair), causing asymmetry in the bond lengths and remarkably different site-specific reactivity [5,7]. Like Si, the carbon atom belongs to Group IV, and organic molecules therefore offer natural bonding compatibility with the Si surface and they are widely used for surface functionalization [8–10]. In particular, multifunctional organic molecules are especially interesting, because one functional group can be used to anchor the molecule to a selected site on the surface, while the other functional groups provide different reaction sites for selective chemistry to occur. For example, Zhu et al. [11] used a series of chain-like bifunctional molecules containing the amine, silane and pyrenyl groups as interconnects between different oxide surfaces and single-walled carbon nanomaterials, while Voue et al. [12] used grafted *N*-hydroxysuccinimidyl ester on a Ge surface for protein detection. Furthermore, Veiseh et al. [13] deployed bifunctional poly(ethylene

* Corresponding author.
E-mail address: tong@uwaterloo.ca (K.T. Leung).

0039-6028/$ – see front matter © 2010 Elsevier B.V. All rights reserved.
doi:10.1016/j.susc.2010.03.011

glycol) polymer to functionalize the surfaces of Fe nanoparticles to make nanoprobes that recognize glioma cells. Finally, Haick and Cahen illustrated different techniques of using bifunctional organic molecules to connect two different surfaces for applications in molecular electronics [14].

In order to understand the relative reactivity of simple organic molecules, particularly on the Si(100)2×1 surface, we have recently conducted a series of studies involving bifunctional molecules. By comparing the reactivities of several common functional groups including halogen atoms (Br, [15] Cl, [16]) hydroxyl (OH) [17], carbonyl (C=O) [17], and carboxylic groups (COOH) [18,19], to a reference group such as ethenyl group (C=C), we obtain qualitative understanding of factors that control their reactivities on the Si(100)2×1 dimer surface. In the present work, we extend our study on bifunctional organic adsorbates on the 2×1 surface to a popular "linker" molecule [20–27], allylamine (CH_2=CH—CH_2—NH_2) [28], which contains one of the most important hydrophilic groups in biological and biochemical sciences, the amino group (NH_2). In the studies of protein and DNA adsorption on metal [25,26,29] and Si surfaces, [20,27] the ethenyl group was used to attach allylamine to the surface while the amino group provided the reaction site to bind to other biological molecules. The surface functionalization by allylamine through the ethenyl group, leaving a free terminal amino group, has in effect changed the native surface and enabled biological reactions to occur, further facilitating biomaterial-mediated tissue responses and cell adhesion [23,30–32].

Several studies on allylamine on Si surfaces have been reported. In particular, Warner et al. [33] and Wang et al. [4] in separate theoretical studies, and Yamada [20], by using high-resolution electron energy loss and Auger electron spectroscopies, showed that functionalization of Si quantum dots and H-terminated Si(111), respectively, by allylamine led to a hydrophilic surface terminated with NH_2 [20,33]. However, a recent Density Functional Theory (DFT) calculation on allylamine adsorption on Si(100) by Prayongpan and Greenlief [34] showed N—H dissociative bonding on a modeled 2×1 surface of a single-dimer Si_9H_{12} cluster, in marked contrast to the previous work on Si(111) [20].

To date, no experimental study has been reported for the adsorption of allylamine on Si(100)2×1. Using X-ray photoelectron spectroscopy (XPS) and thermal desorption spectrometry (TDS), we demonstrate N—H dissociative adsorption of allylamine on the 2×1 surface, in contrast to the expected [2+2] C=C cycloaddition found for molecules containing an ethenyl group on the 2×1 surface. By following the XPS spectra and desorption profiles as a function of temperature, we also show, for the first time, that the dissociatively adsorbed allylamine undergoes further dissociation to propene, ethylene and acetylene and to a N-containing adspecies below 740 K, the latter of which further evolves to form Si nitride at 825 K, where the hydrophobic Si—N(H)—CH_2CH=CH_2 surface in effect becomes a hydrophilic Si—N(H) surface upon annealing. Furthermore, using a double-dimer $Si_{15}H_{16}$ cluster to model the (2×1) surface, we provide a more comprehensive description of plausible adsorption structures by DFT calculations. Despite the more negative calculated adsorption energies found for the multi-dentate adstructures, the unidentate N—H dissociation adspecies is preferred.

2. Experimental and computational details

The experimental setup and procedure for the present work have been described in detail elsewhere [35]. Briefly, a home-built, ultrahigh vacuum dual-chamber system with base pressure better than 1×10^{-10} Torr was used. The upper sample preparation chamber was equipped with an ion-sputtering gun for sample cleaning and a four-grid retarding field optics for characterizing the surface morphology by low energy electron diffraction and surface cleanliness by Auger electron spectroscopy, as well as a gas handling system for sample dosing. The lower analysis chamber housed facilities for XPS and TDS analysis. In particular, an XPS electron spectrometer (VG Scientific CLAM-2), consisting of a hemispherical analyzer of 100 mm mean radius and a triple-channeltron detector, was used to analyze photoelectrons excited by unmonochromatic Al K_α radiation (at 1486.6 eV photon energy) delivered by a twin-anode X-ray source. A differentially pumped 1–300 amu quadrupole mass spectrometer (VG Quadrupole SXP Elite) was used to provide TDS measurements of mass fragments thermally desorbed from the sample. A home-built programmable proportional–integral–differential temperature controller was employed to provide a linear sample heating rate of 2 K s^{-1} [18].

A 10×14 mm^2 Si sample was cut from a single-side polished, p-type (B-doped) Si(100) wafer (0.4 mm thick) with a resistivity of 0.0080–0.0095 Ω cm (Virginia Semiconductors). The sample was first solvent-cleaned and hydrogen-terminated by using a standard RCA method under ambient condition [36]. The sample was then mounted on the sample holder mechanically by using Ta clamps at both ends, with a type-K thermocouple (wrapped in a Ta foil) securely fastened onto the front face at one end of the sample [18]. Detailed descriptions of the sample mounting and preparation procedures were given in our early work [37]. Briefly, the surface was cleaned in the preparation chamber by repeated cycles of Ar ion sputtering for 30 m (at an Ar gas pressure of 4×10^{-5} Torr, 20 mA emission current, and 1.5–2 keV ion beam energy) followed by annealing to 900 K for 5 m by passing a direct current through the sample. The sample was then flash-annealed to 1100 K for 20 s to obtain the 2×1 reconstructed surface. The cleanliness of the surface was verified by the sharpness of the low energy electron diffraction patterns and the lack of contaminant XPS features (e.g. C 1 s and O 1 s).

Allylamine (99.9% purity), a colorless, odorless liquid, was purchased from Sigma-Aldrich and was degassed by several freeze–pump–thaw cycles before exposure to the clean Si(100)2×1 surface. The exposure of the chemical was controlled by backfilling the sample preparation chamber to an appropriate exposure pressure (as monitored by an uncalibrated ionization gauge) using a variable leak valve for a preselected time duration. All exposures were performed at room temperature and reported in units of Langmuir (1 L = 1×10^{-6} Torr s). Unless stated otherwise, a saturation exposure has been used for both temperature-dependent XPS and TDS experiments.

XPS spectra were collected with an acceptance angle of ±4° at normal emission from the Si sample and a constant pass energy of 50 eV, giving an effective energy resolution of 1.4 eV full-width-at-half-maximum (FWHM) for the Si 2p photopeak. The binding energy (BE) scale of the XPS spectra has been calibrated to the Si 2p feature of the bulk at 99.3 eV. After appropriate background subtraction (using the Shirley background), individual XPS spectral components could be fitted with Gaussian–Lorentzian lineshapes by using the CasaXPS software. For temperature-dependent XPS experiments, the sample was flash-annealed to the preselected temperature and allowed to cool back to room temperature before collecting the XPS spectra.

TDS profiles were obtained from the sample, after carefully positioned at 1 mm from the orifice (2 mm dia.) of the differentially pumped housing of the mass spectrometer to ensure that the detected mass fragments originated only from the Si sample [37]. Due to the spatial separation between the thermocouple position and the sampling position viewed by the mass spectrometer, the temperature scale was calibrated by using the temperature of the desorption maximum for recombinative H_2 desorption from Si monohydrides (780 K) [38]. The uncertainty of determining the desorption temperature was estimated to be ±20 K.

Electronic structure calculations were performed using the DFT/B3LYP method [39] with the Gaussian 03 package [40]. The hybrid B3LYP functional, consisting of Becke's 3-parameter gradient-corrected exchange functional [41] and the Lee–Yang–Parr correlation functional [42], has been found to provide generally good agreement with the experimental data for the adsorption of many molecular

systems on Si(100)2×1 [15,18,37]. Moderately sized basis sets, including 6-31G(d), 6-31+G(d), 6-31++G(d), and 6-31++G(d,p), have been used in the present work and were found to give similar optimized geometries, with the larger basis set providing a lower total energy. To simulate the Si surface structure, the cluster model has often been used, with the one-dimer cluster (Si_9H_{12}) [34] giving poorer comparison with the experimental bond lengths and tilting angles [43] than the double-dimer cluster ($Si_{15}H_{16}$) [6,44,45], and higher-order dimer clusters [46]. While higher-order dimer clusters generally give better results, significant increase in the computational effort and time is required. In the present work, we employed the double-dimer cluster to model the Si(100)2×1 surface, because the double-dimer cluster offers a good compromise between accuracy and computational time, while facilitating observation of the dimer buckling effect and investigation of other phenomena related to inter-dimer interactions, which cannot be studied by using just a single-dimer cluster [46]. To obtain an initial guess for the $Si_{15}H_{16}$ cluster, we used a new procedure by first constructing the bulk structure from experimental crystallographic data [43,47] for the Si space group (Fd − 3 m 227) in the Diamond3 crystallographic freeware, and then followed by adding the terminal H atoms and refining the positions of the dimer atoms based on the experimental crystallographic data of the surface [43] in GaussView [40]. The resulting cluster structure was then fully optimized with Gaussian 03 [40]. The present procedure can be easily extended to higher-order dimer clusters and is discussed in more detail elsewhere [48].

In the present work, we also introduced a more systematic method of obtaining the equilibrium geometry of the free chain-like organic molecule (allylamine), before allowing it to become an adsorbate on the surface, by first calculating the total energy as a function of the dihedral angle [48]. By scanning the dihedral angle of the four backbone atoms of allylamine (N→C—C←C) using a small basis set [6-31G(d)] over 360° in 1° steps, we could obtain not only all the local minima for the staggered and eclipsed conformer geometries but also the transition states, which eliminated the risk of missing the true local minimum in the structural optimization procedure. Once the local minima were found with the smaller basis set, they could be used for further optimization by using a larger basis set to provide a more refined geometry. The resulted conformers were combined with that of the $Si_{15}H_{16}$ cluster to be fully optimized, without any geometrical constraint, to obtain the adsorbate–substrate configurations (ASCs). The corresponding adsorption energy, ΔE, was estimated by the difference between the total energy for the optimized structures of the ASCs and the sum of the total energies of a free conformer and the $Si_{15}H_{16}$ cluster. Frequency calculations were also performed for all of the optimized geometries, in order to assure that the local minima correspond to the equilibrium structures and not transition-state structures. All the total energies were obtained without zero-point correction and no basis set superposition error correction was made to ΔE [48].

3. Results and discussion

3.1. DFT computational study of adsorbate–substrate configurations

Fig. 1 shows the optimized free-molecule geometries of two conformers of allylamine, which correspond to two local minima at dihedral angles of 126.0° and 353.0° [48]. Table 1 compares the total energies for the optimized geometries of the conformers for four different basis sets. Not surprisingly, the total energies of the conformers are found to be effectively identical within the limitation of the present calculation, i.e. with a difference less than 0.003 hartree (or 7.88 kJ). Furthermore, the small energy barriers among local minima, with at most 0.006 hartree (or 15.75 kJ), suggest that the conformers are equally probable at room temperature. More complete discussion of the present calculation is given in [48].

Fig. 2 shows plausible ASCs obtained from geometry optimization of allylamine eclipsed (E) conformer (Fig. 1b) and staggered (S) conformer (Fig. 1a), respectively, on the double-dimer $Si_{15}H_{16}$ model surface for Si(100)2×1. Table 1 summarizes the corresponding adsorption energies and total energies for the ASCs calculated by the DFT/B3LYP method for four different basis sets. As expected, the total energies of the ASCs obtained by the larger basis set are more negative than those obtained by the smaller basis set. Furthermore, while the adsorption energies do not appear to follow a particular trend with increasing size of the basis set, the 6-31++G(d,p) basis set generally gives the least negative value. ASC E1 (Fig. 2a) and ASC S1 (Fig. 2d) correspond to unidentate adstructures resulting from N—H dissociation of the E and S conformers, respectively, leading to the formation of Si—N and Si—H bonds on the Si dimer pair. ASC E2 (Fig. 2b) and ASC S2 (Fig. 2e) correspond to similar N—H dissociative products with the dissociated H bonded on a neighboring dimer diagonally across from the Si—N bonding site (cross-dimer). It should be noted that unrestricted B3LYP method has been used to obtain convergence for the open-shell structures of ASCs E2 and S2. Not surprisingly, the adsorption energies for N—H dissociative products are found to be quite similar to one another, with ΔE for ASC E1 (-218.47 kJ mol^{-1}) [S1 (-213.80 kJ mol^{-1})] more negative than that for ASC E2 (-194.95 kJ mol^{-1}) [S2 (-209.71 kJ mol^{-1})], which could be qualitatively attributed to extra energy required for H migration from one dimer to another. Furthermore, ASC E3 (Fig. 2c) and ASC S3 (Fig. 2f) correspond to the respective bidentate adstructures resulting from [2+2] C=C cycloaddition reaction of the ethenyl group of the E and S conformers. The dative bonding between N and the electron-deficient down-atom site of the Si dimer leads to the initial attachment of allylamine to Si through N followed by N—H dissociation and rearrangement to eventually form ASC E1 (S1). The reduction of the π bond (of Si dimer) and the subsequent formation of two Si—C bonds in the cycloaddition reaction has been generally found to produce a less stable adstructure than the corresponding N—H dissociation reaction. In the present case, we also observe a less stable [2+2] C=C cycloaddition product for ASC E3 ($\Delta E = -169.50$ kJ mol^{-1}) than ASC E1. However, a more stable cycloaddition product is found for ASC S3 ($\Delta E = -231.72$ kJ mol^{-1}) than ASC S1, which is likely due to the formation of dative bonding between N and Si through the N electron lone-pair brought about by the proximity of the amino group to the neighboring Si dimer. The remaining ASC E4 or S4 (Fig. 2g) involves simultaneous interactions of both amino and ethenyl groups of either the E or S conformer with the two Si dimer pairs to produce essentially the same [N, C, C] tridentate adstructure. The adsorption energies for the tridentate ASCs (-337.78 kJ mol^{-1} for E4 and -335.14 kJ mol^{-1} for S4) are found to be the most negative among all the ASCs, which suggests that the tridentate ASCs are the most thermodynamically stable adstructures. Despite the most negative values found for the tridentate ASCs, we do not expect these to play a major role, because of the high activation energy needed for multiple bond dissociations (such as N—H and C=C).

It is also of interest to note that the bond lengths for the unidentate ASCs (E1, E2, S1, S2) are found to be essentially unchanged (within 0.01 Å) from those of the free conformers (Fig. 2), and the Si—N bond length (1.75 Å) is also identical for all the unidentate ASCs as well as the tridentate ASCs. For the cycloaddition products, the Si—C bond length (1.95 Å) is essentially the same for both E3 and S3, while the corresponding C=C bond length has changed from 1.34 Å to that of the C—C value (1.58 Å), with the other C—C and C—N bond lengths remaining unchanged, upon [2+2] cycloaddition.

3.2. XPS study of the allylamine adsorption on Si(100)2×1 at room temperature

The XPS spectra of allylamine on Si(100)2×1 have been collected for a number of room-temperature exposures (0.5 L, 2.5 L, 5 L, 10 L,

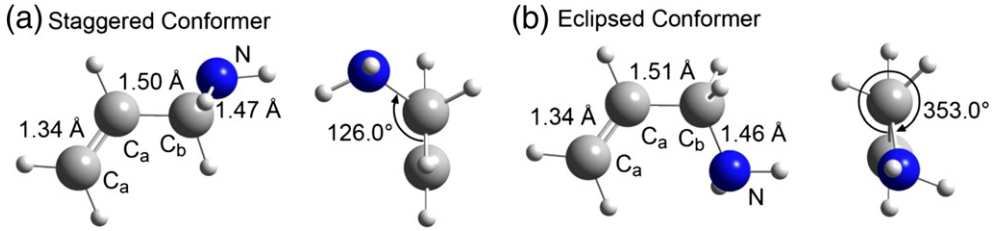

Fig. 1. The equilibrium structures of (a) staggered and (b) eclipsed conformers of allylamine obtained by the DFT/B3LYP/6-31++G(d,p) calculation.

20 L, 50 L, 100 L, and 200 L), and the similarities in the spectral profiles suggest that the predominant adspecies are the same over the range of studied exposures. In Fig. 3, we show representative N 1 s and C 1 s spectra for a low (2.5 L) and a saturation exposure (100 L). Evidently, except for the lower overall intensities, the shapes of both the N 1 s and C 1 s spectra are essentially unchanged from the low to saturation exposure. The single broad N 1 s feature at 398.9 eV BE (with 1.9 eV FWHM) (Fig. 3a, b) can be attributed to Si—N(H)—C←, in good accord with earlier studies that reported N 1 s BE at 398.4–399.1 eV for N—H dissociation products [49–54]. It should be noted that the N 1 s BEs for *tert*-butylamine, diethylamine, and methylethylamine [49], dimethylamine and trimethylamine [52], 1,4-phenylenediamine [53] and other alkylamines [54] adsorbed on Si(100)2×1 or dative bonded to the surface through the electron lone-pair have been reported at 399.5–402.3 eV [49–54]. The present N 1 s assignment is also in good agreement with the N 1 s BE (399.1 eV) for glycine on Si(111)7×7 upon dissociative N—H adsorption [55]. Based on the present assignment, we can rule out the [2+2] C=C cycloaddition ASCs E3 and S3 (Fig. 2) as the plausible adsorption products, because of the lack of N 1 s feature at a higher BE associated with the terminal amino group (399.5–402.3 eV BE) [49–54].

The C 1 s spectra (Fig. 3c, d) are fitted with two broad peaks at 284.6 eV and 286.2 eV BE (with 1.7 eV FWHM). Previous studies showed that the C 1 s BEs for C—N (286.0 eV) and C=C bonds (284.2–285.0 eV) are generally higher than that for Si—C (284.3–283.2 eV) [18,49,50,52,54]. The observed C 1 s features at 284.6 eV (C_a) and 286.2 eV (C_b) can therefore be attributed to the ethenyl C (C=C) and methylene C in the C—N bond, respectively. Furthermore, the approximate relative intensity ratio of 2 to 1 found for C_a 1 s and C_b 1 s is in good accord with the stoichiometric ratio of the ethenyl to methylene C atoms, further supporting our present assignment. The absence of any discernible feature below 284 eV BE confirms that the formation of Si—C bonds, as a result of [2+2] C=C cycloaddition of the ethenyl group, is unlikely and therefore can be used to exclude multi-dentate ASCs (E3, S3, E4, and S4, Fig. 2). This observation is in marked contrast to the formation of a Si—C bond (via saturation of C=C to form an unidentate adstructure) found for allylamine on Si(111) [20] and Si quantum dots [33]. Our XPS data therefore definitively identify the presence of the unidentate N—H dissociation products (ASCs E1, E2, S1, and S2), despite their less negative Δ*E*s than those of the multi-dentate ASCs (Table 1), which suggests that the formation of these unidentate adspecies is kinetically favored.

3.3. Temperature-dependent XPS and TDS studies of thermal evolution products

Fig. 4 shows the XPS spectra of N 1 s and C 1 s regions for a saturation (100 L) room-temperature exposure of allylamine on Si(100)2×1 surface collected upon flash-annealing to different temperatures. The corresponding intensities of individual fitted N 1 s and C 1 s components, relative to the intensity of the Si 2p peak, are also shown as a function of flash-annealing temperature. The N 1 s feature for Si—N(H)—C← at 398.9 eV is found to be remarkably stable, with essentially no reduction in the intensity, up to 565 K (Fig. 4a). From 650 K to 825 K, the N 1 s feature for Si—N(H)—C← has almost completely diminished, while a new feature at 397.7 eV BE emerges and becomes a dominant feature. The intensity of the latter feature remains effectively unchanged upon further flash-annealing to 1090 K. The N 1 s feature at a lower BE can be assigned to Si—NH, present either as a radical or bridge-

Table 1
Adsorption energies (in kJ mol^{-1}), where applicable, and total energies (in hartree), given in square parentheses, of the double-dimer $Si_{15}H_{16}$ cluster, free allylamine staggered (S) and eclipsed (E) conformers, and different adsorbate–substrate configurations (ASCs) obtained by DFT/B3LYP calculations with four different basis sets.

Adsorption energy (kJ mol^{-1}) [Total energy (hartree)]		Basis set			
		6-31G(d)	6-31+G(d)	6-31++G(d)	6-31++G(d,p)
$Si_{15}H_{16}$ cluster		[−4352.059071]	[−4352.071932]	[−4352.073387]	[−4352.091204]
Allylamine conformers	126.0° (S)	[−173.246768]	[−173.259134]	[−173.259364]	[−173.273235]
with dihedral angle	353.0° (E)	[−173.246158]	[−173.258024]	[−173.258229]	[−173.272228]
ASC E1		−232.426903	−223.194018	−223.351836	−218.467199
		[−4525.393756]	[−4525.414967]	[−4525.416687]	[−4525.446641]
ASC E2[a]		−208.870287	−199.721391	−199.812732	−194.952013
		[−4525.384783]	[−4525.406027]	[−4525.407722]	[−4525.437685]
ASC E3		−176.925802	−170.436827	−170.721300	−169.496215
		[−4525.372616]	[−4525.394873]	[−4525.396641]	[−4525.427989]
ASC E4		−357.911757	−343.308043	−343.396943	−337.775590
		[−4525.441550]	[−4525.460716]	[−4525.462410]	[−4525.492083]
ASC S1		−231.644951	−218.431728	−218.559800	−213.795804
		[−4525.414263]	[−4525.414263]	[−4525.415996]	[−4525.445868]
ASC S2[a]		−228.503776	−215.065496	−214.939892	−209.710053
		[−4525.392871]	[−4525.412981]	[−4525.414618]	[−4525.444312]
ASC S3		−253.479344	−234.443786	−234.506536	−231.716837
		[−4525.402384]	[−4525.420361]	[−4525.422070]	[−4525.452694]
ASC S4		−356.311173	−340.394316	−340.418497	−335.137697
		[−4525.441550]	[−4525.460716]	[−4525.462410]	[−4525.492084]

[a] The unrestricted B3LYP functional has been used to take into account of the unpaired electrons of these ASCs.

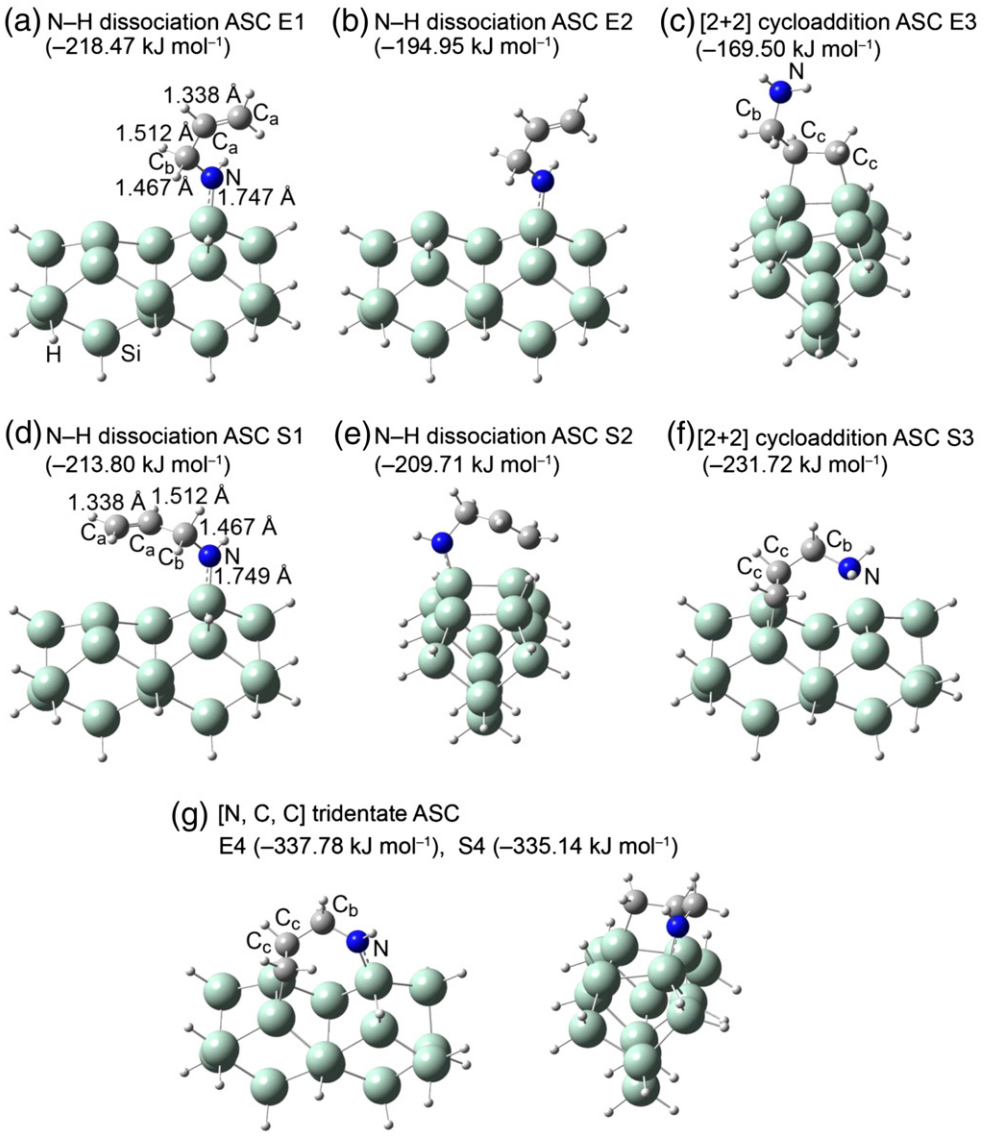

Fig. 2. Optimized geometries of the adsorbate–substrate configurations (ASCs) for eclipsed (a, b, c, g) and staggered conformers (d, e, f, g) of allylamine on a model Si(100)2×1 surface: (a, b, d, e) N—H dissociation, (c, f) [2 + 2] C=C cycloaddition, and (g) [N, C, C] tridentate products. The corresponding adsorption energies calculated with the 6-31++G(d,p) basis set are given in parentheses.

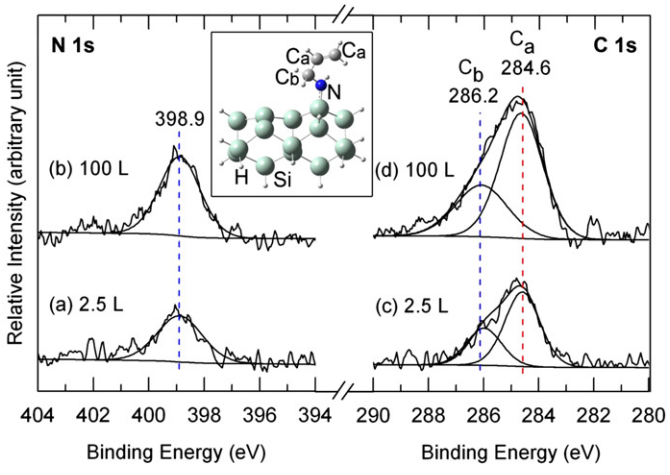

Fig. 3. XPS spectra of C 1 s (right) and N 1 s regions (left) for (a, c) a low (2.5 L) and (b, d) a saturation (100 L) exposures of allylamine on Si(100)2×1 at room temperature. The inset shows a plausible N—H dissociative adstructure with the ethenyl C_a and methylene C_b atoms appropriately identified.

bonded to a second Si atom as Si—N(H)—Si, resulting from C—N bond cleavage of the unidentate N—H dissociation adspecies, e.g. ASC E1. Elimination or replacement of C with an electronegativity (χ) of 2.5 (Pauling scale) [56] with a better electron donor such as Si ($\chi = 1.8$) is expected to increase the partial negative charge of N ($\chi = 3.0$), which in turn causes the corresponding N 1 s feature to appear at a lower BE.

The present assignment for similarly adsorbed NH fragments is also consistent with the BEs (397.2–397.8 eV) for alkylamines and other amino-containing species adsorbed on Si(100) reported previously [49–54]. It is of interest to note that only a relatively minor reduction (24%) in the overall intensity of N 1 s features at 650–740 K is observed (Fig. 4b), which indicates predominant dissociative conversion of unidentate N—H dissociation adspecies into NH-containing fragments on the surface. Furthermore, the lack of relevant N-containing desorption fragments at 650–740 K as illustrated by our TDS data shown below rules out the desorption of any N-containing species from the surface and suggests that the observed reduction corresponds to diffusion of dissociated N (or NH) fragments into the bulk.

Like the N 1 s spectrum, the corresponding C 1 s spectral envelope remains unchanged until the flash-annealing temperature of 565 K

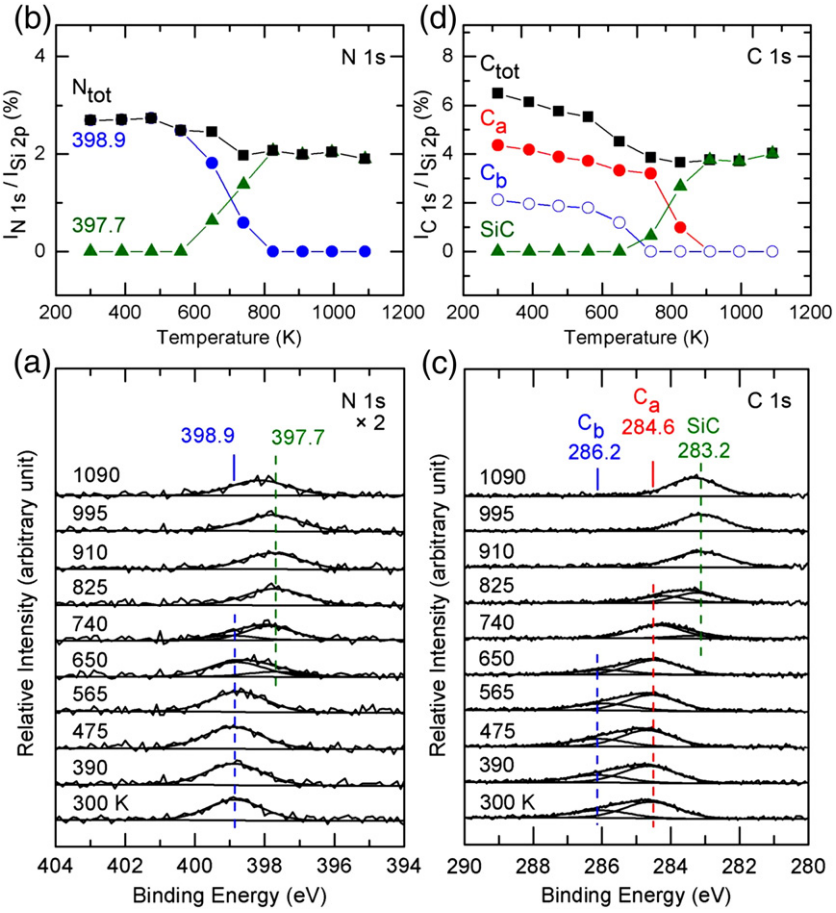

Fig. 4. Temperature-dependent XPS spectra of (a) N 1 s region and (c) C 1 s region for a saturated exposure (100 L) of allylamine on Si(100)2×1 at 300 K, and upon sequential flash-annealing to 390 K, 475 K, 565 K, 650 K, 740 K, 825 K, 910 K, 995 K and 1090 K. Corresponding temperature profiles of the intensities of (b) N 1 s ($I_{N\,1\,s}$) and (d) C 1 s ($I_{C\,1\,s}$) for Si—N(H)—C← at 398.9 eV, Si—NH at 397.7 eV, C_b at 286.2 eV, C_a at 284.6 eV and SiC at 283.2 eV, along with their total intensities N 1 s (N_{tot}) and C 1 s (C_{tot}), all with respect to Si 2p ($I_{Si\,2p}$).

(Fig. 4c) is reached. Between 565 K and 650 K (Fig. 4c), the methylene C_b 1 s peak at 286.2 eV is found to undergo a marked reduction and becomes totally diminished at 740 K (Fig. 4c). As expected, the temperature evolution of C_b 1 s therefore parallels that of the N 1 s feature at 398.9 eV, both of which mark the C—N bond cleavage at 565–740 K. In contrast to the C_b 1 s feature, the intensity of the ethenyl C_a 1 s feature at 284.6 eV has remained unchanged up to the annealing temperature of 740 K, above which dramatic intensity reduction is observed. This reduction in the C_a 1 s intensity continues to 825 K and is complete at 910 K (Fig. 4d). This indicates that above 740 K, the dissociated propenyl species (—$CH_2CH{=}CH_2$) stays on the surface and undergoes further dissociation into smaller fragments (e.g. —CH_2, and —$CH{=}CH_2$) on the surface and/or desorption. Starting at 740 K and becoming more notable at 825 K, the emergence of a new C 1 s feature at 283.2 eV, commonly attributable to SiC, [18,49,50,52,54] is clearly evident (Fig. 4c). The growth of the SiC feature is complete at 910 K, above which no significant change is found (to 1090 K). The growth evolution of the SiC feature is consistent with the proposed thermal dissociation of smaller C-containing fragments into CH_n and finally to C on the surface above 740 K. In contrast to the minor reduction in the total N 1 s intensity, a considerable loss in the total C 1 s intensity (>43%) is found over the flash-annealing temperature range. This larger C 1 s intensity reduction indicates that a significant amount of C has been removed from the surface through the thermal desorption of C-containing adspecies.

In order to determine the desorption products thermally evolved from the adspecies remaining on the surface (as inferred from Fig. 4), TDS experiments were performed. Fig. 5 shows the TDS profiles of selected mass fragments of m/z 2, 26, 27, 28, 39, 41, and 42 for a room-temperature saturation exposure (100 L) of allylamine on Si(100) 2×1. It should be noted that we have also monitored other mass fragments including m/z 17, 30, 31, 56 and 57 but found no detectable intensity. The lack of m/z 56 ($C_3H_5NH^+$) and m/z 57 ($C_3H_5NH_2^+$) signals, corresponding respectively to the base mass and parent mass of allylamine, indicates that the unidentate N—H dissociation adspecies does not desorb molecularly from the surface [28]. Furthermore, the absence of detectable TDS signals for m/z 30 ($CH_2NH_2^+$) and m/z 31 ($CH_3NH_2^+$), corresponding to the base mass of both methylamine and ethylamine and to the parent mass of methylamine, respectively, and for m/z 17 (NH_3^+), corresponding to the parent (and base) mass of ammonia, shows that N-containing adspecies do not desorb from the surface. This observation therefore confirms our earlier hypothesis that N fragments likely diffuse into the bulk (Fig. 4b). For m/z 2 (Fig. 5a), the large desorption feature observed at 780 K can be attributed to the recombinative desorption of H_2 from silicon monohydrides [38]. For the remaining TDS profiles in Fig. 5, a common desorption feature at 580 K has been found for m/z 26, 27, 28, 39, 41 and 42, suggesting a common source. Given that the cracking pattern of propene ($CH_3CH{=}CH_2$) contains m/z 26 ($C_2H_2^+$), m/z 27 ($C_2H_3^+$), m/z 39 ($C_3H_3^+$), m/z 40 ($C_3H_4^+$), m/z 41 ($C_3H_5^+$, base mass) and m/z 42 ($C_3H_6^+$, parent mass) [28], the TDS feature at 580 K could correspond to recombinative desorption of propene, arising from a propenyl radical (•$CH_2CH{=}CH_2$) with H, upon C—N bond cleavage observed at 565–650 K in Fig. 4. The TDS feature of m/z 28 ($C_2H_4^+$, parent and base masses of ethylene) found at 580 K

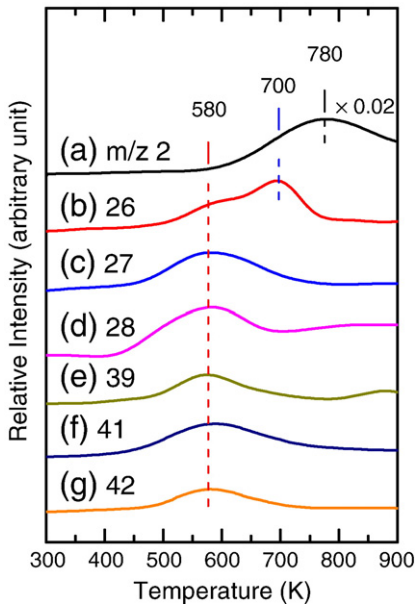

Fig. 5. TDS profiles for selected fragments of m/z (a) 2, (b) 26, (c) 27, (d) 28, (e) 39, (f) 41, and (g) 42 for a saturation (100 L) exposure of allylamine on Si(100)2×1 at room temperature.

suggests desorption of ethylene, the cracking pattern of which also includes m/z 27 ($C_2H_3^+$) and m/z 26 ($C_2H_2^+$). The additional desorption intensities found for m/z 27 and m/z 26 not accountable from desorption from propene could therefore be attributed to ethylene desorption at 580 K. In addition, an additional TDS feature at 700 K is also observed for m/z 26 (Fig. 5b) and not for other mass fragments, which corresponds to desorption of acetylene (with m/z 26 as its parent and base masses), generally found at a similar temperature as reported in earlier studies [17,35].

Fig. 6 summarizes the schematic pathways proposed for the thermal evolution of unidentate N—H dissociation adspecies (e.g., ASC E1). In particular, the unidentate adspecies (Structure I) undergoes N—C bond cleavage (Structure II), producing the propenyl radical (•CH_2—CH=CH_2, Structure IIa, IIc) that either recombines with H and desorbs as propene (pathway b) at 490–685 K (Structure IIb) or stays on the surface with the formation of Si—C bond (pathway c). The propenyl adspecies further dissociates via C—C bond breakage (Structure IId), producing methyl radical (attached to the surface through a Si—C bond) and ethenyl radical (CH_2=CH•, Structure IIe) that desorbs as acetylene at 700 K (Structure IIf). Both pathways (b and c) result in the formation of Si—N(H)—Si that remains stable on the surface (up to our maximum attainable temperature of 1090 K). The unidentate adspecies (Structure I) could also evolve through pathway d with C—C bond cleavage (Structure III) to form ethenyl radical and (•CH_2—NH—Si) adspecies (Structure IV). The ethenyl radical could recombine with H and desorb as ethylene (pathway e) at 490–685 K (Structure IVd) or dehydrogenate as acetylene (pathway f) at 635–755 K (IVb), while the C—N bond cleavage of the remaining methylene amine adspecies could lead to the formation of methylene and methyl adspecies (with Si—C bond formation), respectively, along with Si—N(H)—Si. Given that H

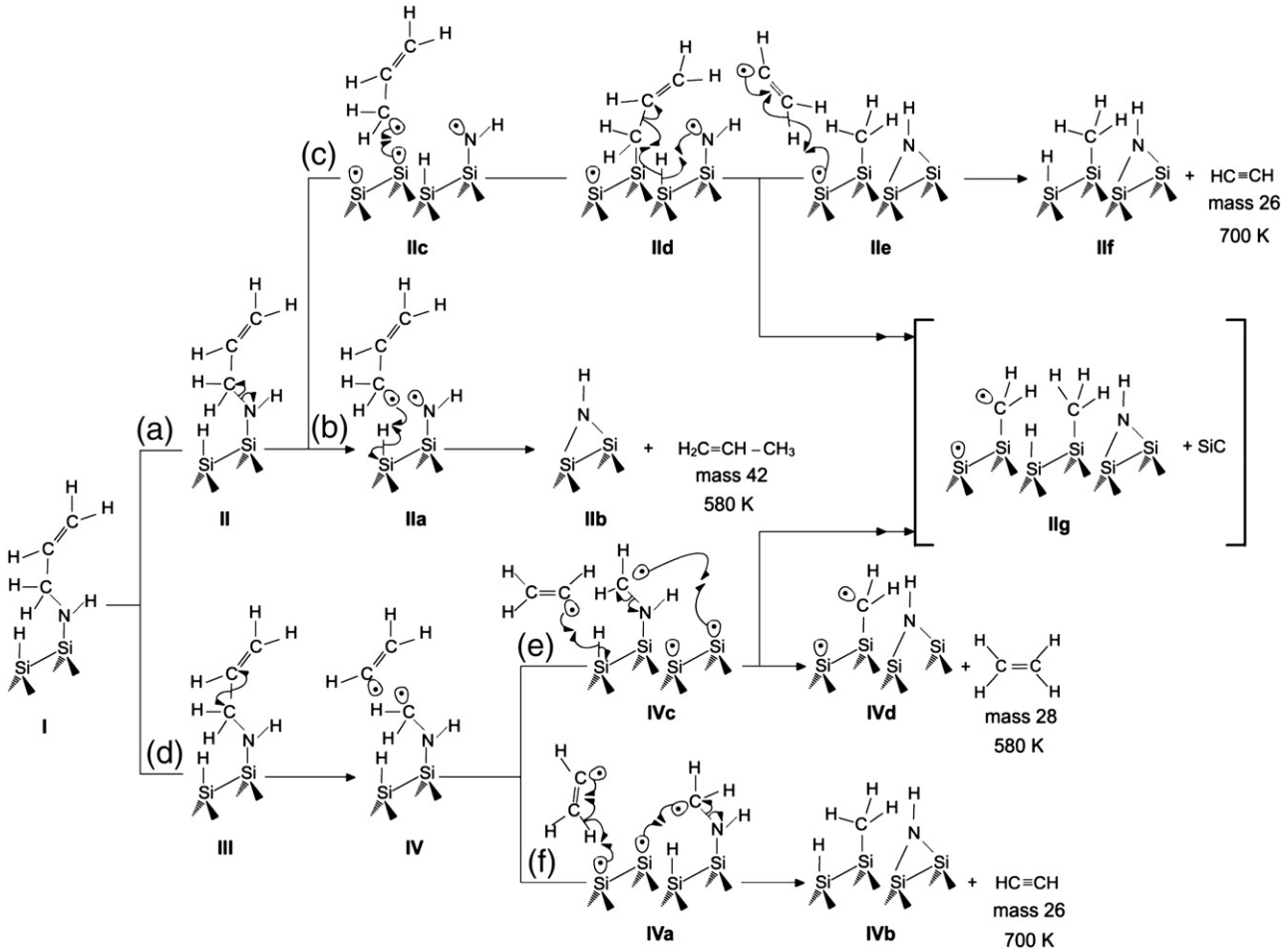

Fig. 6. Schematic model for thermal evolution of an unidentate N—H dissociation adspecies (Structure I), depicting the possible pathways for the formation of Si—N(H)—Si, and propene, ethylene and acetylene, along with surface C-containing fragments (e.g., CH_2, and CH_3).

abstraction involves the breakage of Si—H bond (with a bond dissociation energy of 293 kJ mol^{-1}) [57] to produce ethylene while dehydrogenation involves dissociation of C—H bond (399 kJ mol^{-1}) to produce acetylene, it is therefore not surprising that the desorption maximum of m/z 26 for acetylene occurs at a higher temperature (700 K) than those of m/z 26, 27, and 28 for ethylene (580 K). Furthermore, the similar desorption maxima of m/z 26, 27, 28, 39, 41 and 42 found for propene and ethylene (both at 580 K) are consistent with the similar bond dissociation energies of C—N (356 kJ mol^{-1}) and C—C bonds (385 kJ mol^{-1}) required, respectively, in the formation of propenyl (pathway b) and ethenyl adspecies (pathway e). It should also be noted that the ethenyl radical produced through pathways c (Structure IIe) and e (Structure IVc) could also stay on the surface and undergo total decomposition to form smaller hydrocarbon fragments that give rise to the SiC C 1 s features observed above 700 K (Structure IIg).

4. Concluding remarks

In the present work, we have carried out temperature-dependent XPS and TDS experiments on the room-temperature adsorption of allylamine on Si(100)2×1. Detailed DFT calculations, involving both the eclipsed and staggered conformers of allylamine on a model surface based on the double-dimer $Si_{15}H_{16}$ cluster, have also been employed to interpret our data. Our XPS data show that room-temperature adsorption of allylamine on Si(100)2×1 leads to an unidentate N—H dissociation adspecies, instead of the bidentate [2+2] C=C cycloaddition or [N, C, C] tridentate adspecies. This result is in good accord with the previous work on the adsorption of the amino-containing molecules on Si(100), in which N—H dissociative adsorption through the amino group is found to be the primary process [49–54]. In our earlier work on ethenyl-containing bifunctional molecules (allyl alcohol, allyl aldehyde [17], and acrylic acid [18]) on Si(100)2×1, we show that adsorption proceeds through surface reactions of the hydroxyl [17], carbonyl [17], and carboxyl [18] groups, with the ethenyl group remaining intact. The present work also shows that the amino group is more reactive than the ethenyl group and that N—H dissociative adsorption is the preferred route. The nature of the surface bonding for allylamine on Si(100)2×1 is, however, in marked contrast to that found for the adsorption of allylamine on Si(111) [20] and Si quantum dots [33], which show an unidentate adspecies bonding through saturation of one of the ethenyl C atoms with the amino group intact. This difference suggests that the surface structure itself [i.e. (100) vs (111)] plays an important role in the adsorption of bifunctional molecules.

In addition to the formation of propene desorbate, our TDS data on allylamine also show common desorbates, such as ethylene and acetylene, arising from thermal evolution of the ethenyl group, that are also found for allyl alcohol, allyl aldehyde [17], and acrylic acid on Si(100) [18]. The formation of Si—N(H) and/or Si—N above 650 K is also confirmed with the presence of the respective N 1 s features in our temperature-dependent XPS study. Surface functionalization of Si(100)2×1 by allylamine therefore offers a number of interesting control opportunities, by in effect converting the double-bond of a Si dimer of the 2×1 surface to a C=C double-bond of the "dangling" ethenyl group after N—H dissociative adsorption, which effectively replaces silicon chemistry by organic chemistry to better serve the role of an organic linker molecule. By annealing the functionalized surface to 825 K, the organic moiety is desorbed and the surface is transformed to a N or NH terminated Si surface, in effect converting a hydrophobic surface to a hydrophilic surface. Such a conversion can be easily achieved by controlling the annealing temperature.

Finally, our DFT calculations based on the double-dimer cluster have significantly extended the calculation of Prayongpan and Greenlief (based on the single-dimer cluster) [34]. The use of the double-dimer cluster to model the 2×1 surface has allowed us to uncover new [N, C, C] tridentate ASCs (with $\Delta E = -335.14$ to -337.77 eV), which are considerably more stable than the N—H dissociation ASCs (with $\Delta E = -194.95$ to -218.47 eV), in contrast to the [2+2] cycloaddition ASCs (with $\Delta E = -169.50$ to -231.72 eV) being only slightly more stable. Despite these considerably more stable tridentate ASCs, our experimental result implicates the unidentate N—H dissociation adspecies as the only viable product, which suggests that the formation of such an adstructure is kinetically favored on the Si(100)2×1 surface. This latter result shows that a sufficiently large cluster is necessary to model the 2×1 surface in order to provide a more comprehensive picture and new insights to the intricate silicon surface chemistry of bifunctional organic molecules.

Acknowledgment

This work was supported by the Natural Sciences and Engineering Research Council of Canada. The calculations were performed, in part, at the WHALE cluster of the Shared Hierarchical Academic Research Computing Network supported by the governments of Canada and the province of Ontario. We are grateful to Drs. Marcel Nooijen, Michael Chong, Jake Fisher and Youngku Sohn for helpful discussions of various relevant aspects of computational methods and organic chemistry.

References

[1] R.A. Wolkow, Ann. Rev. Phys. Chem. 50 (1999) 413.
[2] M.A. Filler, S.F. Bent, Prog. Surf. Sci. 73 (2003) 1.
[3] T.R. Lefwich, A.V. Teplyakov, Surf. Sci. Rep. 63 (2008) 1.
[4] X. Wang, R.Q. Zhang, T.A. Niehaus, T. Frauenheim, J. Phys. Chem. C 111 (2007) 2394.
[5] J. Yoshinobu, Prog. Surf. Sci. 77 (2004) 37.
[6] J. Li, Y.-Q. Qu, K.-L. Han, G.-Z. He, Surf. Sci. 586 (2005) 45.
[7] C.B. Duke, Chem. Rev. 96 (1996) 1237.
[8] N. Sheppard, Ann. Rev. Phys. Chem. 39 (1988) 589.
[9] S.M. Barlow, R. Raval, Surf. Sci. Rep. 50 (2003) 201.
[10] Z. Ma, F. Zaera, Surf. Sci. Rep. 61 (2006) 229.
[11] J. Zhu, M. Yudasaka, M. Zhang, D. Kasuya, S. Iijima, Nano Lett. 3 (2003) 9.
[12] M. Voue, E. Goormaghtigh, F. Homble, J. Marchand-Brynaert, J. Conti, S. Devouge, J. De Coninck, Langmuir 23 (2007) 949.
[13] O. Veiseh, C. Sun, J. Gunn, N. Kohler, P. Gabikian, D. Lee, N. Bhattarai, R. Ellenbogen, R. Sze, A. Hallahan, J. Olson, M. Zhang, Nano Lett. 5 (2005) 6.
[14] H. Haick, D. Cahen, Acc. Chem. Res. 41 (2008) 359.
[15] X.J. Zhou, Q. Li, Z.H. He, X. Yang, K.T. Leung, Surf. Sci. 543 (2003) L668.
[16] X.J. Zhou, K.T. Leung, Surf. Sci. 600 (2006) 468.
[17] M. Ebrahimi, K.T. Leung, Surf. Sci. 603 (2009) 1203.
[18] M. Ebrahimi, J.F. Rios, K.T. Leung, J. Phys. Chem. C 113 (2009) 281.
[19] M. Ebrahimi, J.M. Chong, K.T. Leung, J. Phys. Chem. C 114 (2010) 2947.
[20] T. Yamada, Curr. Appl. Phys. 6S1 (2006) 26.
[21] V. Krishnamurthy, I.L. Kamel, Polym. Chem. 27 (1989) 1211.
[22] M. Lejeune, F. Brétagnol, G. Ceccone, P. Colpo, F. Rossi, Surf. Coat. Technol. 200 (2006) 5902.
[23] A. Harsch, J. Calderon, R.B. Timmons, G.W. Gross, J. Neurosci. Meth. 98 (2000) 135.
[24] G.L. Chen, W.J. Zhao, S.H. Chen, M.Y. Zhou, W.R. Feng, W.C. Gu, S.Z. Yang, Appl. Phys. Lett. 89 (2006) 121501.
[25] Z. Zhang, W. Knoll, R. Förch, Surf. Coat. Technol. 200 (2005) 993.
[26] Q. Chen, R. Förch, W. Knoll, Chem. Mater. 16 (2004) 614.
[27] A.L. Hook, H. Thissen, J. Quinton, N.H. Voelcker, Surf. Sci. 602 (2008) 1883.
[28] P.J. Linstrom, W.G. Mallard (Eds.), NIST Mass Spec Data Center, "Mass Spectra" in NIST Chemistry WebBook, NIST Standard Reference Database Number 69, National Institute of Standards and Technology, Gaithersburg, 2005, http://webbook.nist.gov.
[29] M. Morra, C. Cassinelli, A. Carpi, R. Giardino, M. Fini, Biomed. Pharmacotheraphy 60 (2006) 365.
[30] J.D. Whittle, R.D. Short, C.W.I. Douglas, J. Davies, Chem. Mater. 12 (2000) 2664.
[31] L. Tang, Y. Wu, R.B. Timmons, J. Biomed. Mater. Res. 42 (1998) 156.
[32] M. Tatoulian, F. Brétagnol, F. Arefi-Khonsari, J. Amouroux, O. Bouloussa, F. Rondelez, A. John Paul, R. Mitchell, Plasma Proc. Polym. 2 (2004) 38.
[33] J.H. Warner, A. Hoshino, K. Yamamoto, R.B. Tilly, Angew. Chem. Int. Ed. 44 (2005) 4550.
[34] P. Prayongpan, C.M. Greenlief, Surf. Sci. 603 (2009) 1055.
[35] X.J. Zhou, Q. Li, K.T. Leung, J. Phys. Chem. B 110 (2006) 5602.
[36] W. Kern, D.A. Puotinen, RCA Rev. 31 (1970) 187.
[37] Q. Li, K.T. Leung, Surf. Sci. 479 (2001) 69.
[38] C.C. Cheng, J.T. Yates Jr., Phys. Rev. B 43 (1991) 4041.
[39] W. Kohn, L.J. Sham, Phys. Rev. 140 (1965) A1133.
[40] M. J. Frisch, G. W. Trucks, H. B. Schlegel, G. E. Scuseria, M. A. Robb, J. R. Cheeseman, J. A. Montgomery Jr., T. Vreven, K. N. Kudin, J. C. Burant, J. M. Millam, S. S. Iyengar, J. Tomasi, V. Barone, B. Mennucci, M. Cossi, G. Scalmani, N. Rega, G. A. Petersson, H. Nakatsuji, M. Hada, M. Ehara, K. Toyota, R. Fukuda, J. Hasegawa, M. Ishida, T.

Nakajima, Y. Honda, O. Kitao, H. Nakai, M. Klene, X. Li, J. E. Knox, H. P. Hratchian, J. B. Cross, V. Bakken, C. Adamo, J. Jaramillo, R. Gomperts, R. E. Stratmann, O. Yazyev, A. J. Austin, R. Cammi, C. Pomelli, J. W. Ochterski, P. Y. Ayala, K. Morokuma, G. A. Voth, P. Salvador, J. J. Dannenberg, V. G. Zakrzewski, S. Dapprich, A. D. Daniels, M. C. Strain, O. Farkas, D. K. Malick, A. D. Rabuck, K. Raghavachari, J. B. Foresman, J. V. Ortiz, Q. Cui, A. G. Baboul, S. Clifford, J. Cioslowski, B. B, Stefanov, G. Liu, A. Liashenko, P. Piskorz, I. Komaromi, R. L. Martin, D. J. Fox, T. Keith, M. A. Al-Laham, C. Y. Peng, A. Nanayakkara, M. Challacombe, P. M. W. Gill, B. Johnson, W. Chen, M. W. Wong, C. Gonzalez, J. A. Pople, Gaussian 03, Gaussian, Inc., Wallingford, CT, 2005.
[41] A.D. Becke, J. Chem. Phys. 98 (1993) 5648.
[42] C. Lee, W. Yang, R.G. Parr, Phys. Rev. B 37 (1988) 785.
[43] R. Felici, I.K. Robinson, C. Ottaviani, P. Imperatori, P. Eng, P. Perfetti, Surf. Sci. 375 (1997) 55.
[44] X. Lu, X. Xu, N. Wang, Q. Zhang, M.C. Lin, J. Phys. Chem. B 105 (2001) 10069.
[45] C. Mui, M.A. Filler, S.F. Bent, C.B. Musgrave, J. Phys. Chem. B 107 (2003) 12256.
[46] H.R.R. Santos, M.J. Ramos, J.A.N. Ferreira Gomes, C. R. Chimie 8 (2005) 1461.
[47] G. Celotti, D. Nobili, P. Ostoja, J. Mater. Sci. 9 (1974) 821.
[48] A. Radi, M.Sc. Thesis, University of Waterloo, Waterloo, Canada (2009).
[49] J.B. Wu, Y.W. Yang, Y.F. Lin, H.T. Chiu, J. Phys. Chem. B 108 (2004) 1677.
[50] X.P. Cao, R.J. Hamers, J. Phys. Chem. B 106 (2002) 1840.
[51] E.K. Hlil, L. Kubler, J.L. Bischoff, D. Bolmont, Phys. Rev. B 35 (1987) 5913.
[52] X. Cao, R.J. Hamers, J. Am. Chem. Soc. 123 (2001) 10988.
[53] Th. Kugler, U. Thibaut, M. Abraham, G. Folkers, W. Göpel, Surf. Sci. 260 (1992) 64.
[54] X. Cao, R.J. Hamers, J. Vac. Sci. Technol. B 20 (2002) 4.
[55] L. Zhang, A. Chatterjee, M. Ebrahimi, K.T. Leung, J. Chem. Phys. 130 (2009) 121103.
[56] F.A. Carey, Organic Chemistry, 3rd Edition, McGraw-Hill, Toronto, 1996.
[57] "Bond Dissociation Energies" by Y.-R. Luo, in CRC Handbook of Chemistry and Physics, 88th Edition (Internet Version 2008), edited by D. R. Lide, CRC Press/Taylor and Francis, Boca Raton.